Food Chemistry: X 34 (2026) 103572

Contents lists available at ScienceDirect

Food Chemistry: X

journal homepage: www.sciencedirect.com/journal/food-chemistry-x

Effect of amylose content in corn starch on the rheological properties, 3D printability, and in vitro digestive properties

Ya'nan Wang [a,b], Shuangqi Tian [a,b,*], Mengsi Cui [a,b], Zixuan Liu [a,b], Zhanpeng Liu [a,b], Zehua Liu [a,b], Jing Lu [c]

[a] College of Grain and Food, Henan University of Technology, Zhengzhou 450001, China
[b] Food Laboratory of Zhongyuan, Luohe 462300, China
[c] Department of Molecular Sciences, Swedish University of Agricultural Sciences, PO Box 7015, SE-75007 Uppsala, Sweden

ARTICLE INFO

Keywords:
High amylose corn starch
3D food printability
Starch digestibility

ABSTRACT

High amylose corn starch (HACS) is a promising functional food ingredient, resisting digestion. Amylose content matters for starch gelatinization, gel formation, and 3D printing. It also links to the content of resistant starch (RS). Achieving optimal 3D printing with ideal digestion resistance challenges starch-based food printing. This study sought the optimal amylose range balancing these traits. Four corn starches (amylose: 28.68%–70.06%) were tested for rheology, printing accuracy, RS, structural features. HACS-1946 (58.84% amylose) had low printing deviation (6.59% in length) and high RS (33.93%, compared to 10.09% in 28.68% amylose normal starch), balancing resistance and formability. In contrast, HACS-K130 (66.13%) and HACS-1945 (70.06%) had significant printing defects from rapid retrogradation. Gelatinization and 3D printing reduced RS by disrupting crystallinity, but only changed physical aggregation. These findings suggest moderate amylose content balances formability and nutritional benefits, offering insights for developing starch-based 3D products with controllable digestibility, precision, and functionality.

1. Introduction

3D printing, an additive manufacturing process, employs computer digitalization to create three-dimensional objects through 3D modeling, slicing, data processing, and layer-by-layer printing (He et al., 2020). A range of materials, including chocolate (You et al., 2023), dough (Masbernat et al., 2021), minced meat (Dong et al., 2020), and starch gel (Kaur et al., 2022), have been investigated as potential food inks to meet diverse application needs. The successful application of food 3D printing is critically dependent on the rheological performance of the food ink, which must exhibit not only sufficient fluidity for smooth extrusion but also rapid solidification after deposition to maintain structural fidelity. This necessity has established the investigation of the physicochemical properties of food ingredients and their compatibility with printing processes as a paramount research focus in the field.

Starch, the primary component of cereals, is a promising 3D printing material due to its unique viscoelasticity, including shear-thinning, thixotropy, and the ability to form self-supporting gels. Starch typically acts as a pseudoplastic non-Newtonian fluid. This property is mainly determined by the molecular interactions between amylose and amylopectin. During gelatinization, starch exhibits pronounced shear-thinning behavior, which facilitates nozzle extrusion in 3D printing (Jo et al., 2021). Conversely, retrogradation induces crystalline structure formation, stabilizing printed geometries (Liu et al., 2019).

The relative proportion of amylose to amylopectin in starch is a key factor determining its gel rheological properties and the final printing result. Amylose builds a strong network that provides mechanical integrity (Rong et al., 2023), while the branched amylopectin increases system viscosity. Their relative proportion is the key determinant of the starch paste's rheological properties. It has been shown that a gradient of amylose content in starch has a non-linear modulating effect on 3D printing performance. Specifically, systems with more than 50% of amylose content show a significant increase in storage modulus (G'), which increases extrusion resistance and causes printing discontinuities due to rapid water evaporation (Liu, Chen, et al., 2023). On the contrary, formulations with less than 30% of amylose content display excellent fluidity, but struggle to maintain complex structures because of insufficient network crosslinking (Liu et al., 2024).

* Corresponding author at: College of Grain and Food, Henan University of Technology, Zhengzhou 450001, China.
E-mail address: tianshuangqi@haut.edu.cn (S. Tian).

https://doi.org/10.1016/j.fochx.2026.103572
Received 14 September 2025; Received in revised form 3 January 2026; Accepted 19 January 2026
Available online 20 January 2026

High amylose corn starch (HACS), a natural type-2 resistant starch (RS2) characterized by more than 50% amylose content, which promotes the formation of dense, enzyme-resistant crystalline structures, offers multiple advantages: resistance to high temperatures, low solubility, delayed glucose release, prebiotic activity, and high dietary fiber content (Wen et al., 2022). However, its relatively high gelatinisation temperature imposes certain limitations on its practical application. Existing treatments such as high-pressure heating, microwave irradiation (Tian et al., 2023), and alkaline treatment effectively reduce gelatinization temperature and enhance gelation.

Current research have shown that the decoupling relationship between amylose content and 3D printing precision has become a key bottleneck in the transformation and application of starch-based functional materials (Cheng, Gu, et al., 2024). However, a significant research gap exists in this field. It is still unclear how different levels of amylose content simultaneously affect 3D printing accuracy and starch digestibility. Specifically, the influence of amylose content on crystallinity (which affects digestibility) and gelation (which impacts printability) is unclear. Additionally, the dynamic changes in starch's molecular and crystalline structures during gelatinization and printing are still not well understood. This lack of insight into the multiscale structural evolution severely limits the precise design and application of starch-based functional materials in the field of food 3D printing.

This study used four commercially available corn starches differing in amylose content: Normal corn starch (NS, 28.68% amylose), HACS-1946 (58.84% amylose), HACS-K130 (66.13% amylose), and HACS-1945 (70.06% amylose). The investigation focused on elucidating the impact of amylose content on rheological properties, 3D printing performance, and digestibility characteristics. The findings illustrate how amylose content affects the transformation of starch-based materials from native starch to gelatinized starch gels and finally to 3D printed products. This research offers novel insights into the molecular design of starch-based materials for 3D food printing applications.

2. Materials and methods

2.1. Materials and reagents

NS (moisture content: 12.45%, amylose content: 28.68%) was purchased from Xinxiang Xinliang Grain and Oil Processing Co., Ltd. (Henan, China); HACS-1945 (moisture content: 13.42%, amylose content: 70.06%), HACS-K130 (moisture content: 10.44%, amylose content: 66.13%), HACS-1946 (moisture content: 9.67%, amylose content: 58.84%) were purchased from Chuan Yin Xiang Yu Biotechnology Co., Ltd. (Beijing, China). Apparent amylose content was determined by iodine colorimetry. D-glucose (GOPOD Format) assay kit was purchased from Megazyme International Ireland (Bray, Wicklow, Ireland). Amyloglucosidase (Cat. No. A7095) and pancreatin from porcine pancreas (Cat. No. P7545) were procured from Sigma-Aldrich Chemical Co. (St. Louis, MO, USA). All other chemicals and reagents were of analytical grade.

2.2. Preparation of starch samples

Starch sample (100.0 ± 0.5 mg) was dispersed in 1.0 mL of anhydrous ethanol and 9.0 mL of NaOH solution (1.0 M) in a 150 mL Erlenmeyer flask. The slurry was boiled in a water bath with shaking at 100 rpm for 10 min. Subsequently, after cooling, the slurry was stained with iodine and the absorbance was determined at 720 nm. The amylose content of all samples has been determined and is indicated in Section 2.1.

The methodology employed in this study exhibits subtle deviations from the protocol described by Shi et al. (2024). Starch paste was prepared by mixing each starch with distilled water to obtain 20% (*w/v*) starch suspension. Considering the distinct crystalline structures and gelatinization requirements, different heating methods were applied. Starch suspension of NS was heated to 95 °C for 20 min in a water bath (DK-98-II Tianjin Tester Instrument Co., Ltd., Tianjin, China). In contrast, as per previous processing protocols for gelatinized high amylose starch (Li et al., 2025), the suspensions of HACS-1945, HACS-1946, and HACS-K130 were first preheated in a boiling water bath for 20 min with continuous stirring to promote dispersion. The preheated starch suspensions were gelatinized for 20 min at 121 °C in a high-temperature autoclave (YXQ-LS, Shanghai Boxun Industrial Co., Ltd., Shanghai, China). This ensures all starch samples reach a similar gelatinization state. It also avoids bias from incomplete gelatinization when comparing 3D printing performance. The gelatinized starch gels were removed and cooled to room temperature for later use. For the samples of NS, HACS-1945, HACS-1946, and HACS-K130, the gelatinized starch samples were respectively designated as NS-G, HACS-1945-G, HACS-1946-G, and HACS-K130-G.

2.3. 3D printing

Gelatinized gel samples were 3D-printed using the FOODBOT-S2Pro 3D food printer (Shiyin Technology Co. Ltd., Hangzhou, China). A standardized letter "P" model (22 × 35 × 5 mm) was used to evaluate printing properties, assessing extrusion stability, shape retention at directional changes, and path fidelity through straight lines, right angles, and curves. The extrusion column temperature was set to 25 °C. A 0.84 mm diameter plastic nozzle was used. The layer height was set at 0.7 mm. The printing speed (nozzle travel speed) was 15 mm/s to ensure uniform paste extrusion. The length, width, and height of letter samples were measured with a vernier caliper. Length was the maximum vertical distance of vertical lines. Width was the maximum horizontal distance of horizontal lines. Height referred to the stacked thickness along the *Z*-axis. Each sample was printed and measured three times. Printing deviation was calculated using Eq. (1). The 3D-printed starch samples were subjected to freeze-drying and named NS-D, HACS-1945-D, HACS-1946-D, and HACS-K130-D.

$$\text{Printing deviation value}(\%) = \frac{\text{Actual measured value} - \text{Theoretical model value}}{\text{Theoretical model value}} \times 100 \quad (1)$$

2.4. Thermal properties

Thermal properties of NS, HACS-1945, HACS-1946, and HACS-K130 were measured by a differential scanning calorimeter (DSC 6000, Perkin Elmer, Con- necticut, USA) as described by Jiang et al. (2010) with minor modifications. Starch samples (10.0 mg, db) and distilled water (30 μL) was sealed in a stainless-steel pan, equili- brated overnight at 4 °C, and then heated at a rate of 10 °C/min from 20 °C to 160 °C. A sealed empty pan was used as the reference. Onset (To), peak (Tp), and conclusion (Tc) temperatures and enthalpy change (ΔH) of starch gelatinization were calculated using Pyris software (Perkin Elmer, Connecticut, USA).

2.5. Pasting properties

Pasting properties of Starch were measured by a Rapid Visco Analyzer (RVA 4800, Perten Instruments, Stockholm, Sweden) according to the method of Gu et al. (2024). For regular pasting, starch (3.36 g, db) was weighed into an aluminum canister and suspended in 25 mL of deionized water and stirred with a plastic paddle to prevent the formation of lumps. Starch suspension was equilibrated at 50 °C for 1 min, heated to 95 °C at a rate of 12 °C/min, held at 95 °C for 2.5 min, cooled to 50 °C at 12 °C/min, and held at 50 °C for 2 min. Throughout the analysis, the paddle speed was set to 160 rpm, except for the first 10 s at 960 rpm.

For high-temperature pasting, a 12% starch suspension (28.00 g) was equilibrated at 50 °C for 1 min, heated from 50 °C to 140 °C at 12 °C/min, held at 140 °C for 2.5 min, cooled to 50 °C at 12 °C/min, and maintained at 50 °C for 2 min. The pasting temperature (PT), peak viscosity (PV), trough viscosity (TV, the minimum viscosity at 95/140 °C), breakdown viscosity (BV, peak-trough viscosity), final viscosity (FV, viscosity at 50 °C) and setback (SB, final-trough viscosity) were calculated.

2.6. Gel texture properties

The texture properties of the starch gel samples were analyzed using the modified method of Bai et al. (2022). Modified method was suitable for the specific requirement of the experiment. Starch paste prepared according to section 2.2 will be immediately transferred into the sealed plastic container with internal diameter of 29.0 mm and height of 20.0 mm to prevent moisture loss and stored at 4 °C for 24 h. This method was modified to suit the specific requirement of the experiment. After being brought to room temperature for 1 h, the samples were tested using a TA-XT Plus Texture Analyzer (Stable Micro System Ltd., Godalming, UK) with a cylindrical probe (P/0.5R). The pretest, test, and posttest speeds were all set to 1.00 mm/s, compression ratio of 25%, trigger force at 5.0 g. Time interval between tests was 3 s. The TPA indicators recorded included hardness, springiness, cohesiveness, gumminess, chewiness, and resilience.

2.7. Rheological properties

The rheological properties of pastes were determined by a dynamic rheometer (HAAKE MARS60, Thermo Fisher Scientific Inc., USA) with parallel plate geometry of 35 mm diameter (1 mm gap). Under the application of a constant strain of 1%, the sample subject to a frequency sweep test over a broad frequency range from 0.1 Hz to 20 Hz. Throughout this examination, G', the loss modulus (G"), and the loss factor (tan δ) were analyzed. The loss factor, tan δ, is defined as the proportionality between G" and G', expressed as their ratio (tan δ = G"/G'). In addition, a steady-state shear scan was performed to examine the rheological behavior of the sample applied with a steady shear. This scan was carried out over a shear rate range of 0.01 s^{-1} to 100 s^{-1}. Throughout the shear scan, both the apparent viscosity (η) and the shear rate (γ) were meticulously recorded to assess the rheological performance of the sample.

2.8. Scanning electron microscopy

The microstructure of native, gelatinized and 3D-Printed starch samples were determined by scanning electron microscopy (Quanta 250 FEG, TEI Co., Ltd. American). The lyophilized samples passed through 100 mesh sieve were glued onto the conductive adhesive of sample tray with double sided adhesive and then sprayed with gold. The microstructure of starch granules was observed and photographed under accelerating voltage of 3 kV.

2.9. X-ray diffraction

The crystalline structure and relative crystallinity of the lyophilized powder were characterized using an X-ray diffractometer (MiniFlex 600, Rigaku, Japan). Scans were performed over a 2θ range of 5° to 40° at a rate of 2°/min. The relative crystallinity was determined through profile fitting using JADE 6.0 software by applying Pseudo-Voigt functions to separate the crystalline and amorphous components, and was calculated as the corresponding integrated area ratio, following the procedure reported by Meng et al. (2025). A consistent fitting protocol ensured comparability across all samples.

2.10. Fourier transform infrared spectroscopy

Native, gelatinized, and 3D-printed starch samples were mixed with potassium bromide (1:100, mg/mg) and ground in a mortar. Samples requiring freeze-drying were first lyophilized, then fully ground, homogenized, and pressed into tablets. Subsequently, the prepared uniform and transparent tablets were recorded using a Fourier Transform Infrared Spectrometer (Nicolet 6700, Thermo Fisher Scientific, USA). According to Cheng, He, et al. (2024), the range of wavenumber was controlled from 400 cm^{-1} to 4000 cm^{-1}, resolution of 4 cm^{-1} and 32 scans were taken.

2.11. In vitro starch digestibility

The in vitro digestibility of native, gelatinized, and 3D-printed starch samples was determined using the method described by Englyst et al. (1992) and Jiang et al. (2025), with minor modifications. Starch (0.1 g, db) was mixed with 6.0 mL of sodium acetate buffer (0.1 M, pH 5.2) containing porcine pancreatic (6720 U of amylase) and amyloglucosidase (15.5 U) in a 50 mL polypropylene centrifuge tube. The tube was placed into a 37 °C water bath shaker and incubated at 140 rpm. The sample was collected at 0 min, 20 min, and 120 min respectively. Each sample was inactivated by adding 66% ethanol, and then centrifuged at 3000 rpm for 10 min. Subsequently, 100 μL of the supernatant was mixed with 3 mL of GOPOD, and the mixture was incubated in a water bath at 50 °C for 30 min. The absorbance was measured at 510 nm. Starch digested within 20 min was categorized as rapidly digestible starch (RDS), starch digested between 20 and 120 min as slowly digestible starch (SDS), and starch remaining after 120 min as RS. The calculation was performed using Eq. (2).

$$GLU(\%) = \frac{A_t \times V_t \times c \times D}{A_s \times W} \times 100 \quad (2)$$

where A_t is the absorbance of the test solution at 510 nm; V_t is the total volume of the test solution; c is the concentration of the standard solution (mg glucose/mL, glucose oxidase-peroxidase kit); D is the dilution factor; A_s is the absorbance of the standard solution at 510 nm; W is the weight of the sample used for analysis (mg), which can be corrected for moisture content using Eqs. (3)–(5).

$$RDS(\%) = (G_{20} - FG) \times 0.9 \quad (3)$$

$$SDS(\%) = (G_{120} - G_{20}) \times 0.9 \quad (4)$$

$$RS(\%) = TS - RDS - SDS \quad (5)$$

where FG is the free glucose content and TS is the total starch content (%, db) of the sample.

2.12. Statistical analysis

All experiments were performed at least in duplicate. Analysis of variance (ANOVA) was performed based on Duncan's multiple range test ($p < 0.05$) using the IBM SPSS Statistics 21 software (IBM Corp.,

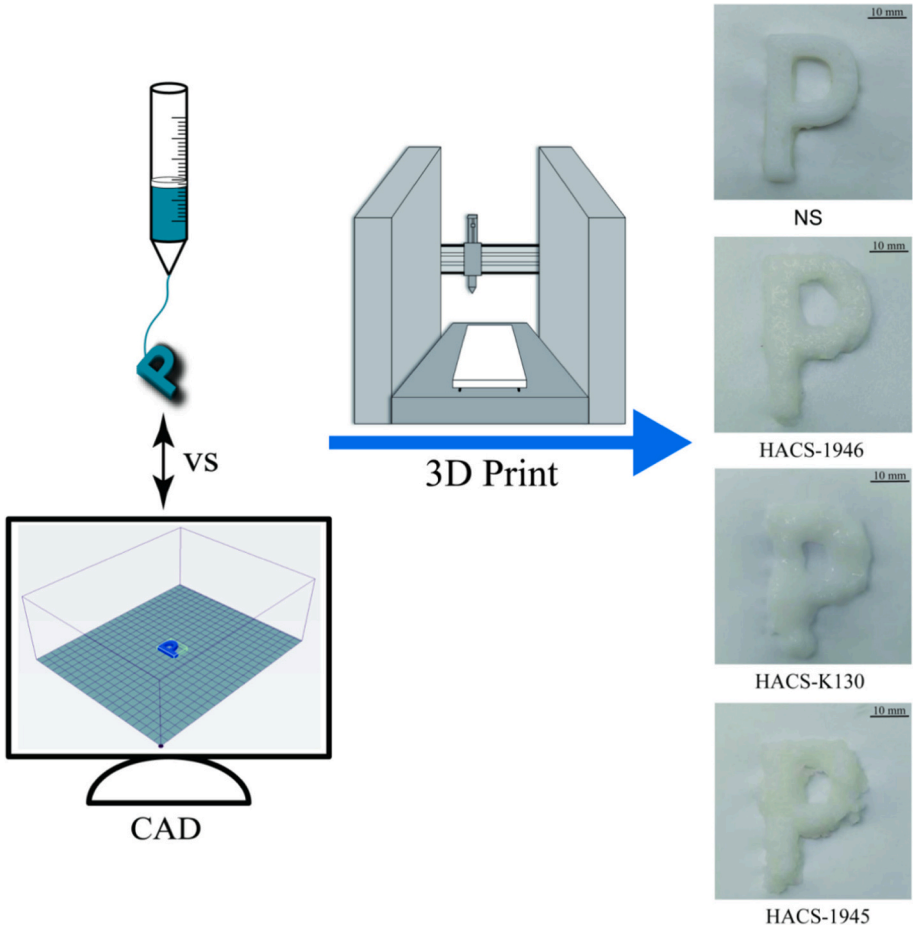

Fig. 1. Images of four 3D-printed corn starch products.

Armonk, USA). The data are reported as mean ± standard deviation. Statistical analysis was performed using the software Origin 2024 (Origin Lab Co., Northampton, USA).

3. Results and discussion

3.1. 3D printing morphological characteristics

As shown in Fig. 1, the "P" shape produced by 3D printing corn starch with different amylose contents. NS and HACS-1946 yielded complete, self-supporting 3D structures with sharp definition, indicating high printing precision. Their extrusion was smooth and uninterrupted, resulting in samples free from breaks or collapse. Conversely, HACS-K130 and HACS-1945 performed poorly, suffering from issues such as gel hardening, nozzle clogging, line breaks, and failed shape formation. This led to substantial deviations from the intended design, especially pronounced at right-angle corners.As shown in Table 1 and Fig. 2, the quantitative assessment of printing accuracy supports the previous observations.The evaluation of 3D-printed samples was conducted using absolute values of length, width, and height deviations (Cai et al., 2023). The results showed that as amylose content rose, dimensional deviations increased and printing accuracy decreased.Importantly, all HACS samples demonstrated negative deviations in the height direction, with the degree of these deviations showing a positive correlation with the

Table 1
Comparison of 3D-printed dimensions for four corn starch samples and target model specifications.

Sample	Length/mm	Width/mm	Height/mm
CAD	22.00 ± 0.00^{d}	35.00 ± 0.00^{e}	5.00 ± 0.00^{b}
NS	22.12 ± 0.07^{d}	35.55 ± 0.17^{d}	5.22 ± 0.08^{a}
HACS-1946	23.45 ± 0.13^{c}	37.38 ± 0.15^{c}	4.37 ± 0.08^{c}
HACS-K130	25.40 ± 0.01^{b}	38.22 ± 0.01^{b}	4.35 ± 0.06^{c}
HACS-1945	28.88 ± 0.08^{a}	46.36 ± 0.18^{a}	3.71 ± 0.03^{d}

Note: Results are presented as mean ± standard deviation. Within a column of each group, data bearing different superscript letters indicate a significant difference.

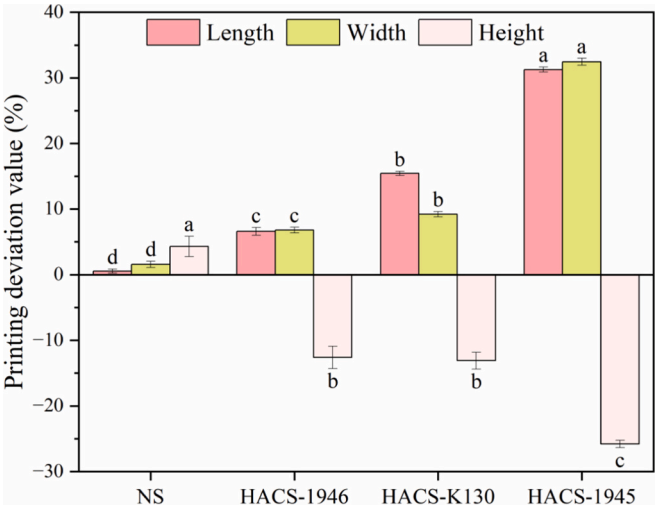

Fig. 2. Printing deviation values for 3D-printed samples of four corn starches.

amylose content.This phenomenon can be explained by the rapid retrogradation of the starch gel during the printing process.Due to their molecular regularity, amylose chains tend to recrystallize more (Ning et al., 2025).Consequently, HACS experienced rapid molecular rearrangement and hardening during printing, leading to gel contraction. This contraction caused the actual extruded volume to be lower than the intended model volume (Cheng et al., 2023).

The observed printing defects are directly linked to material properties. For instance, severe right-angle deformation in HACS-1945 and HACS-K130 correlated with high gel hardness (Table 4) and a high elastic modulus (Fig. 4A). This excessive rigidity hindered material flow during rapid printhead direction changes. Additionally, strong retrogradation increased extrusion resistance. In contrast, NS exhibited the best dimensional accuracy (22.12 × 35.55 × 5.22 mm), with all errors within acceptable limits. Its superior printability originated from a balanced property profile: moderate gel hardness, good interlayer adhesion, and optimized, shear-thinning viscoelasticity. This combination enabled smooth extrusion and accurate shape retention after deposition. In summary, higher amylose content accelerates gel retrogradation. This increases rigidity and reduces plasticity, thereby impairing control over extrusion volume and 3D printing precision.

3.2. Thermal properties

Thermal property parameters of gelatinization (To, Tp, Tc, and ΔH) of four corn starches, along with the DSC curves were listed in Table 2 and Fig. 3A. As shown in the DSC thermograms, the heat absorption peaks of NS were sharp and symmetric, while those of HACS-1946, HACS-K130 and HACS-1945 were flat and asymmetric. Further analysis of the thermal parameters showed that To, Tp, and Tc generally increase as amylose content rises, whereas ΔH decreases. The Tp and Tc values of HACS samples are higher than those of NS, consistent with the results of viscosity characteristics in Table 2. HACS starch molecules form stronger hydrogen bonds, resulting in a more stable crystal structure. Breaking this stable structure requires higher energy, so higher temperatures are needed during gelatinization to break the intermolecular hydrogen bonds, which directly leads to the increase in Tp and Tc. The essence of gelatinization is the process of destroying the crystalline regions of starch particles during heating. ΔH reflects the energy required for starch gelatinization, and its magnitude is directly related to the number of crystalline regions in the starch granules. The higher ΔH values observed in NS directly reflect a higher proportion of crystalline domains in its granules (Guan et al., 2023), a conclusion consistent with the higher relative crystallinity derived from X-ray diffraction data (Fig. 4). In contrast, the crystalline structure of HACS samples exhibits higher stability: on one hand, this makes the gelatinization process more difficult; on the other hand, it further explains why HACS requires higher heating temperatures (i.e., higher Tp and Tc) to disrupt the crystalline structure and achieve complete gelatinization.

Table 2
Thermal and pasting properties of four corn starches.

Sample	To (°C)	Tp (°C)	Tc (°C)	ΔH (J/g)
NS	70.42 ± 0.05^{c}	77.39 ± 0.12^{c}	88.89 ± 0.24^{b}	12.74 ± 1.01^{a}
HACS-1946	71.07 ± 0.70^{c}	82.21 ± 1.41^{b}	114.54 ± 1.13^{a}	7.73 ± 0.37^{b}
HACS-K130	78.75 ± 0.60^{b}	101.71 ± 0.01^{a}	116.39 ± 0.74^{a}	6.06 ± 0.62^{bc}
HACS-1945	81.60 ± 0.66^{a}	101.19 ± 0.50^{a}	114.97 ± 1.07^{a}	5.38 ± 0.16^{c}

Note: Results are presented as mean ± standard deviation. Within a column of each group, data bearing different superscript letters indicate a significant difference.

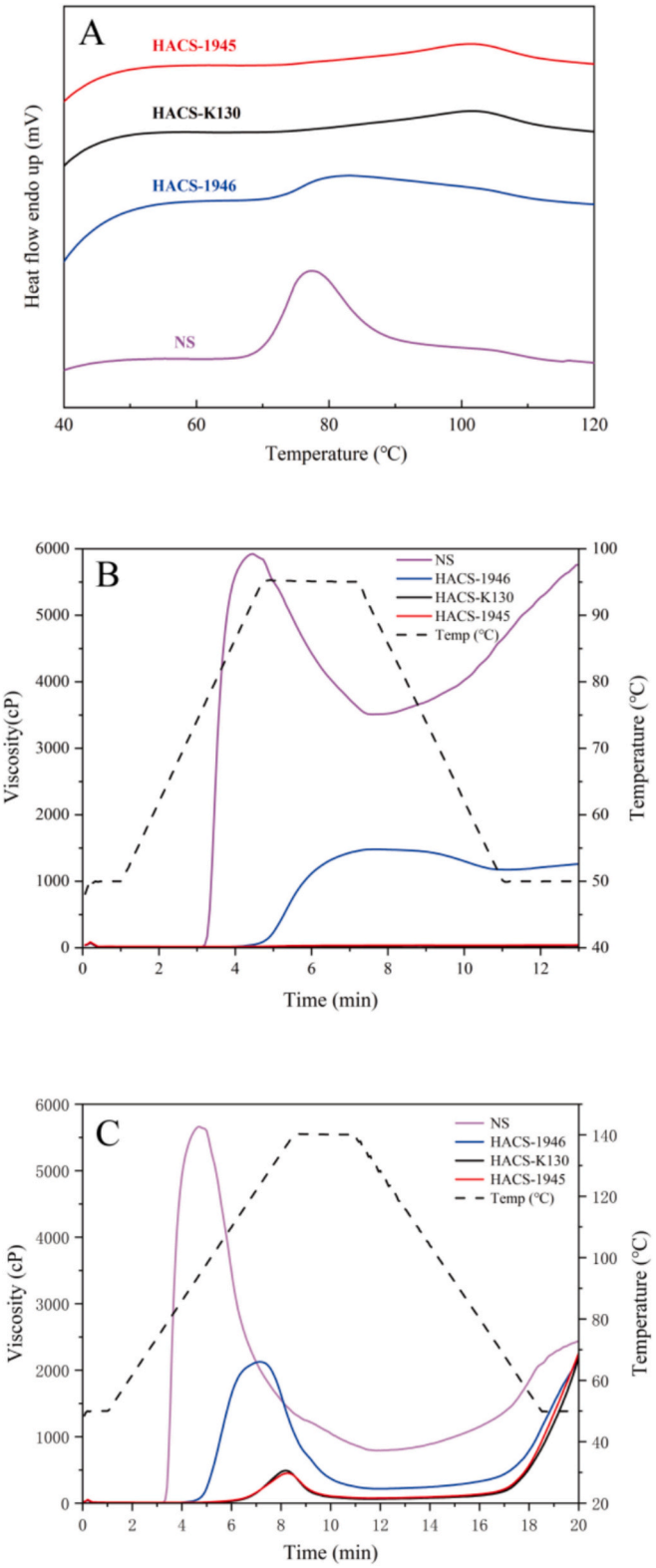

Fig. 3. Thermal and pasting properties of four corn starches. (A)Thermal-transition curves of four corn starches; (B) Pasting curves of corn starch from 50 °C–95 °C-50 °C heating profile; (C) Pasting curves of corn starch from 50 °C–140 °C-50 °C heating profile.

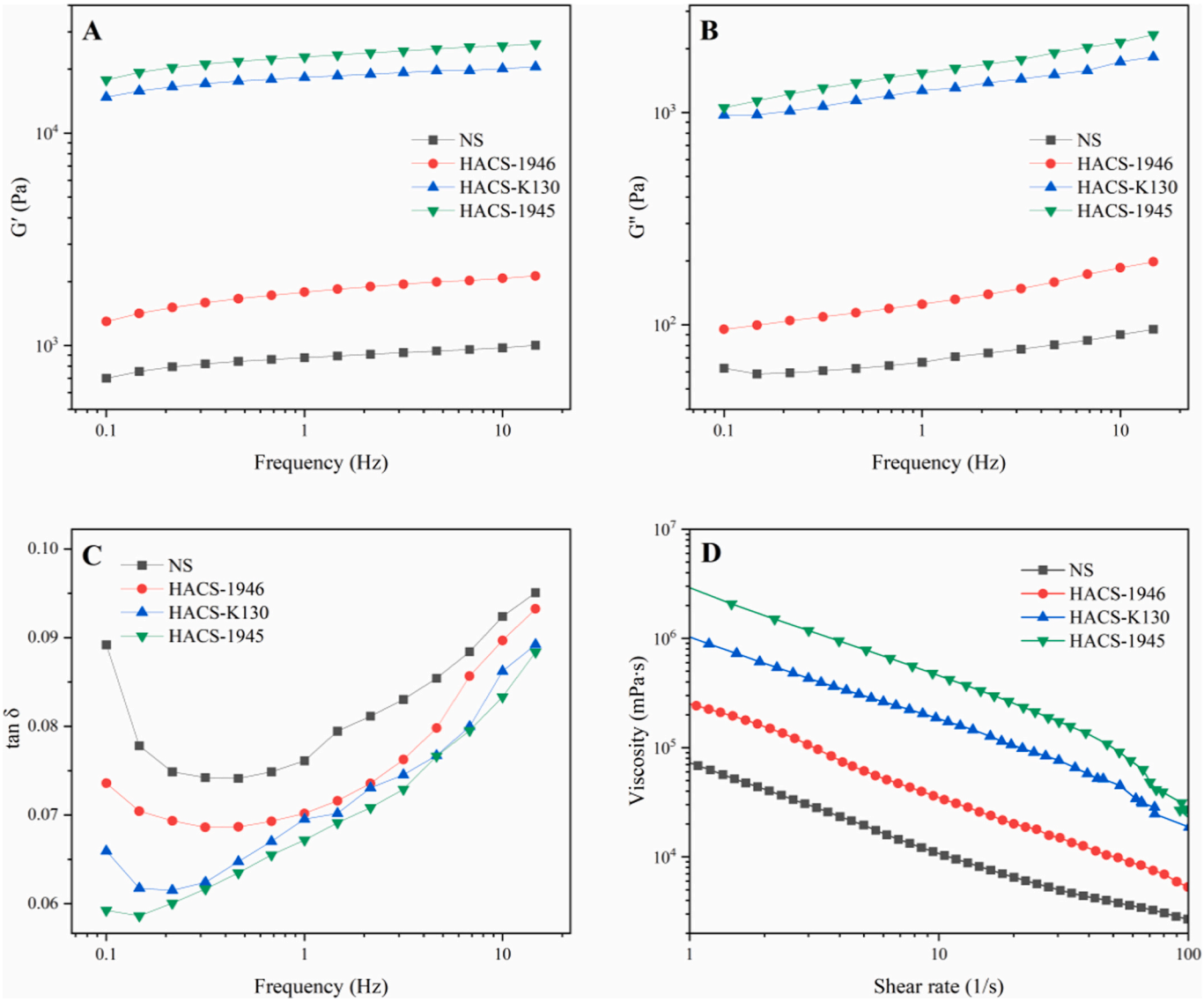

Fig. 4. Rheological behavior of four corn starches. (A) storage modulus; (B) loss modulus; (C) loss factor; (D) apparent viscosity.

Table 3
Pasting properties of four corn starches under conventional (50 °C–95 °C-50 °C) and high-temperature (50 °C–140 °C-50 °C) heating cycles.

Sample	PT (°C)	PV (cP)	TV (cP)	BV (cP)	FV (cP)	SB (cP)
50°C–95 °C-50 °C						
NS	75.85 ± 0.00^{b}	5817.00 ± 14.9^{a}	3501.50 ± 13.44^{a}	2315.50 ± 13.65^{a}	5678.50 ± 11.24^{a}	2177.00 ± 9.89^{a}
HACS-1946	94.13 ± 0.60^{a}	1594.50 ± 23.40^{b}	1296.00 ± 20.36^{b}	298.50 ± 3.41^{b}	1415.50 ± 22.28^{b}	119.50 ± 19.09^{b}
HACS-K130	–	20.00 ± 1.41^{c}	17.00 ± 1.41^{c}	3.00 ± 0.00^{c}	25.00 ± 2.83^{c}	8.00 ± 1.41^{b}
HACS-1945	–	34.00 ± 2.83^{c}	30.50 ± 3.54^{c}	3.50 ± 0.71^{c}	39.50 ± 3.54^{c}	9.00 ± 0.00^{b}
50°C–140 °C-50 °C						
NS	76.70 ± 0.57^{c}	5898.50 ± 3.35^{a}	817.00 ± 3.67^{a}	5081.50 ± 2.99^{a}	2575.00 ± 1.02^{ab}	1758.00 ± 9.34^{c}
HACS-1946	94.35 ± 0.57^{b}	2129.00 ± 5.66^{b}	217.50 ± 0.71^{b}	1911.50 ± 4.95^{b}	2387.00 ± 4.10^{b}	2169.50 ± 4.31^{b}
HACS-K130	121.15 ± 0.00^{a}	495.50 ± 9.19^{c}	65.50 ± 3.50^{d}	430.00 ± 5.66^{c}	2737.00 ± 10.87^{a}	2671.50 ± 12.92^{a}
HACS-1945	121.55 ± 0.55^{a}	469.50 ± 26.16^{c}	75.00 ± 2.83^{cd}	394.50 ± 2.89^{c}	2768.00 ± 10.72^{a}	2693.00 ± 10.46^{a}

Note: Results are presented as mean ± standard deviation. "-", not determined (no pasting peak). Within a column of each group, data bearing different superscript letters indicate a significant difference.

3.3. *Pasting properties*

Pasting characteristics can predict a material's printability and the quality of the printed product (Shi et al., 2024). Viscosity changes can be used to characterize the gelatinization properties of starch, predict the printability of materials, and the quality of printing. As shown in Fig. 3B, C and Table 3, NS exhibited a complete gelatinization curve with significant changes below 95 °C, featuring a PV of 5817.00 cP, and a high

BV value (2315.50 cP), indicating strong shear thinning capability. This allows it to reduce viscosity through shear force during printing extrusion, enabling smooth flow, consistent with the results of minimal printing deviation and complete forming. In contrast, HACS-1946 showed a slowly rising viscosity curve with only a slight increase, maintaining stability until the measurement ends and exhibiting moderate overall viscosity changes, with a PV of 1594.50 cP. Meanwhile, HACS-K130 and HACS-1945 displayed no significant viscosity fluctuations during the entire 95 °C testing process, with PV values as low as 20.00 cP and 34.00 cP, respectively. This phenomenon may be attributed to the intact crystalline structure of amylose under normal temperature and pressure, which hinders the water absorption and swelling of amylopectin within starch granules (Zhong, Qu, et al., 2022). Since HACS did not fully gelatinize at 95 °C, high-temperature, high-pressure RVA was used to measure its gelatinization characteristics.

When the RVA insulation temperature increases from 95 °C to 140 °C, the gelatinization characteristics of HACS undergo significant changes. At 140 °C, as the content of amylose increases, PV, TV, and BV gradually decrease, while FV, SB, and PT correspondingly increase (Guo et al., 2024), leading to further particle expansion, enhanced thermal stability, increased viscosity, and faster retrogradation rates. For food 3D printing, high viscosity of the printing material can cause material blockage in the nozzle, thereby affecting the accuracy of the printed model's shape. Moderate recovery (such as HACS-1946) can enhance the structural stability of the printed object, while excessive recovery leads to printing defects.

3.4. Gel texture properties

As shown in Table 4, the textural properties of gels derived from four types of corn starch with varying amylose contents, including indicators such as hardness, adhesiveness, elasticity, cohesiveness, gumminess, chewiness, and resilience. Hardness, a critical textural parameter, was closely linked to starch extrusion performance and 3D-printed products' self-supporting ability. HACS-1945 gel (605.90 g) showed significantly higher hardness than NS gel (274.25 g), with hardness increasing significantly as amylose content rose. From a molecular perspective, excessively high hardness hindered gel extrusion through 3D printing nozzles post-gelatinization, causing discontinuous lines and design deviations. This stemmed from rapid amylose retrogradation: gelatinized starch gels underwent aging reactions, forming ordered, compact amylose structures that increase hardness—consistent with 3D printing results. Adhesiveness was critical for interlayer bonding: higher values reduced delamination. NS gel (3.60 mJ) showed superior adhesiveness and printing accuracy, while HACS-1945 (1.35 mJ) exhibited poor bonding, impairing print quality. Higher amylose content negatively impacted 3D printing properties via reduced adhesiveness. Cohesiveness, reflecting molecular binding, was significantly higher in NS (0.79) than high amylose starches. Gels with high amylose content exhibited poor cohesiveness (Yu et al., 2016). This demonstrated that a high amylose content reduced the ability of starch gels to bind water molecules, negatively impacting the cohesiveness of hydrogels.

During starch gelatinization to gel formation, amylose molecules spontaneously organized into double-helix structures and assembled into crystalline arrangements. This ordered structure enhanced gel mechanical strength, as HACS-1945 gel exhibited higher G' than other samples (Fig. 4). However, this impeded 3D printing extrusion, risking failures and poor formability. Elasticity depended on starch structure and water content. NS resisted retrogradation and syneresis, retaining moisture to show the highest elasticity. Compared to HACS-1945, HACS-K130, and HACS-1946 gels, NS gel had superior self-supporting ability due to higher adhesiveness and elasticity. Overall, balancing amylopectin/amylose ratios was critical for high-performance 3D printing ink. NS gel showed the lowest printing deviation (Fig. 2), validating this conclusion.

3.5. Rheological properties

Rheological properties were basic parameters for characterizing 3D printing performance of starch-based materials, and rheological behavior of food ink was important to realize accurate and controllable 3D food printing (Cheng et al., 2022). As shown in Fig. 4A, B, and C, the variation of G', G", and tan δ with shear frequency for four corn starch gels. Within the linear viscoelastic region, all gel samples exhibited $G' > G''$ and $\tan\delta < 1$, indicating that the gel systems displayed solid-like elastic behavior, which is necessary for 3D-printed objects shape stability. Additionally, G' and G" of all gel systems increased with rising shear frequency, and their tan δ values exhibited obvious frequency dependence, common in weak gel systems (Li et al., 2021). Notably, amylose content positively correlates with G' and G", but negatively correlates with tan δ. G' and G" increase as frequency and amylose content rise. These effects are attributed to the increased amylose content, which promotes the swelling of starch granules and intermolecular cross-linking, thereby forming a more compact three-dimensional gel network(Zhang et al., 2024). This phenomenon aligns with the report by Zhong et al., 2023 that high-amylose starch gels exhibit higher G′, which is attributed to the enhanced elasticity of the gel network due to effective entanglement of solubilized amylose molecules.

However, a high G′ can cause extrudate swelling, which consequently increases the width of the printed strands (Cheng, Yuqing, et al., 2024). However, excessively high G' values in HACS-1945 and HACS-K130 made the starch gel extrusion flow performance decrease significantly. Expansion or even fracture could easily occur during extrusion, resulting in significant dimensional deviations between the printed product and the target model (Fig. 2). When the amylose content increased, NS and HACS-1946 starch-based gels exhibited the lowest G" at the same frequency, meaning minimal system energy dissipation during cycling. This is likely due to branched starch regulating amylose rearrangement, which affects the distribution of intermolecular and intramolecular forces (Fang et al., 2020). In terms of viscoelastic equilibrium, a high tan δ value helps retain shape in 3D-printed products. In contrast (Al-Muslimawi et al., 2013), HACS gels have lower tan δ values, showing flow characteristics similar to solids.This is due to rapid degradation after gelatinization. Molecular chains form tightly ordered networks through hydrogen bonds, leading to a sharp increase in system stiffness (Saqib Gulzar et al., 2023). This increases extrusion resistance, which can result in fractures and molding failures.

As shown in Fig. 4D, All samples exhibited shear-thinning behavior (Liu, Ling, et al., 2023). High shear in the nozzle reduces ink viscosity for smooth extrusion. After extrusion, the shear effect stops, and viscosity quickly recovers. This helps maintain filament structure and dimensional stability (Liu et al., 2018). This occured because shear forces

Table 4
Gel texture properties of four corn starches.

Sample	Hardness/g	Adhesiveness/mJ	Chewiness	Springiness	Cohesiveness	Gumminess	Resilience
NS	274.25 ± 2.00^{d}	3.60 ± 0.01^{c}	205.39 ± 0.57^{b}	0.97 ± 0.00^{a}	0.79 ± 0.01^{a}	212.96 ± 0.14^{c}	0.43 ± 0.01^{a}
HACS-1946	315.10 ± 1.82^{c}	1.40 ± 0.04^{a}	116.03 ± 2.55^{c}	0.72 ± 0.01^{c}	0.51 ± 0.02^{c}	161.30 ± 0.33^{d}	0.22 ± 0.02^{b}
HACS-K130	466.08 ± 1.58^{b}	2.93 ± 0.36^{b}	219.76 ± 23.63^{b}	0.81 ± 0.05^{b}	0.58 ± 0.03^{b}	269.78 ± 1.60^{b}	0.25 ± 0.01^{b}
HACS-1945	605.90 ± 3.61^{a}	1.35 ± 0.09^{a}	285.33 ± 15.57^{a}	0.85 ± 0.04^{b}	0.55 ± 0.00^{bc}	335.10 ± 1.97^{a}	0.24 ± 0.01^{b}

Note: Results are presented as mean ± standard deviation. Within a column of each group, data bearing different superscript letters indicate a significant difference.

induced breakdown of the starch gel network and drove directional rearrangement of starch chains. In the shear rate range of 1–100 s^{-1} relevant to printing, the apparent viscosities of HACS-1945 and HACS-K130 were significantly higher than those of NS and HACS-1946. This is due to hydrogen bonding interactions and intermolecular entanglements from high-amylose starch, which stabilize the internal gel network (Obadi et al., 2023). However, higher viscosity requires more driving pressure to overcome extrusion resistance during printing. Excessive resistance can cause material adhesion to the feed tube and nozzle blockage, resulting in poor extrusion, filament breakage, and dimensional deviations (Jiang et al., 2019). This phenomenon highlights the dual effect of amylose content on 3D printing performance. The higher amylosecontent is beneficial to the formation of printing products due to the higher G′, whilst the starch paste ink could be difficult to extrude due to the concomitant high viscosity.

3.6. Scanning electron microscopy

As shown in Fig. 5, SEM images of four native starches, four gelatinized starches and four 3D-printed starches with different amylose contents. The NS granules exhibited smooth and intact surfaces without wrinkles, appearing polygonal with multiple flat planes or edges. Most granules are relatively large, though some displayed small pits on their surfaces, presumably resulting from enzymatic activity during starch granule biosynthesis. In contrast, HACS-1946, HACS-K130, and HACS-1945 predominantly exhibited smooth and plump spherical or elliptical morphologies. Numerous fine particles agglomerated into uneven clusters, and the abundance of elongated particles increases significantly with rising amylose content (Wei et al., 2025). These morphological features aligned with the XRD results. After gelatinization and 3D printing, the granular morphology of the four corn starches underwent significant transformation, shifting from their original granular structure to an irregular block-like architecture (Yan et al., 2019). During gelatinization, high temperature and pressure induced dissolution of starch granules, releasing substantial amylose molecules that were highly prone to retrogradation. This led to amylose aggregation and rearrangement into irregular resistant starch networks. Compared to gelatinized starch, 3D-printed starch exhibited a more compact and

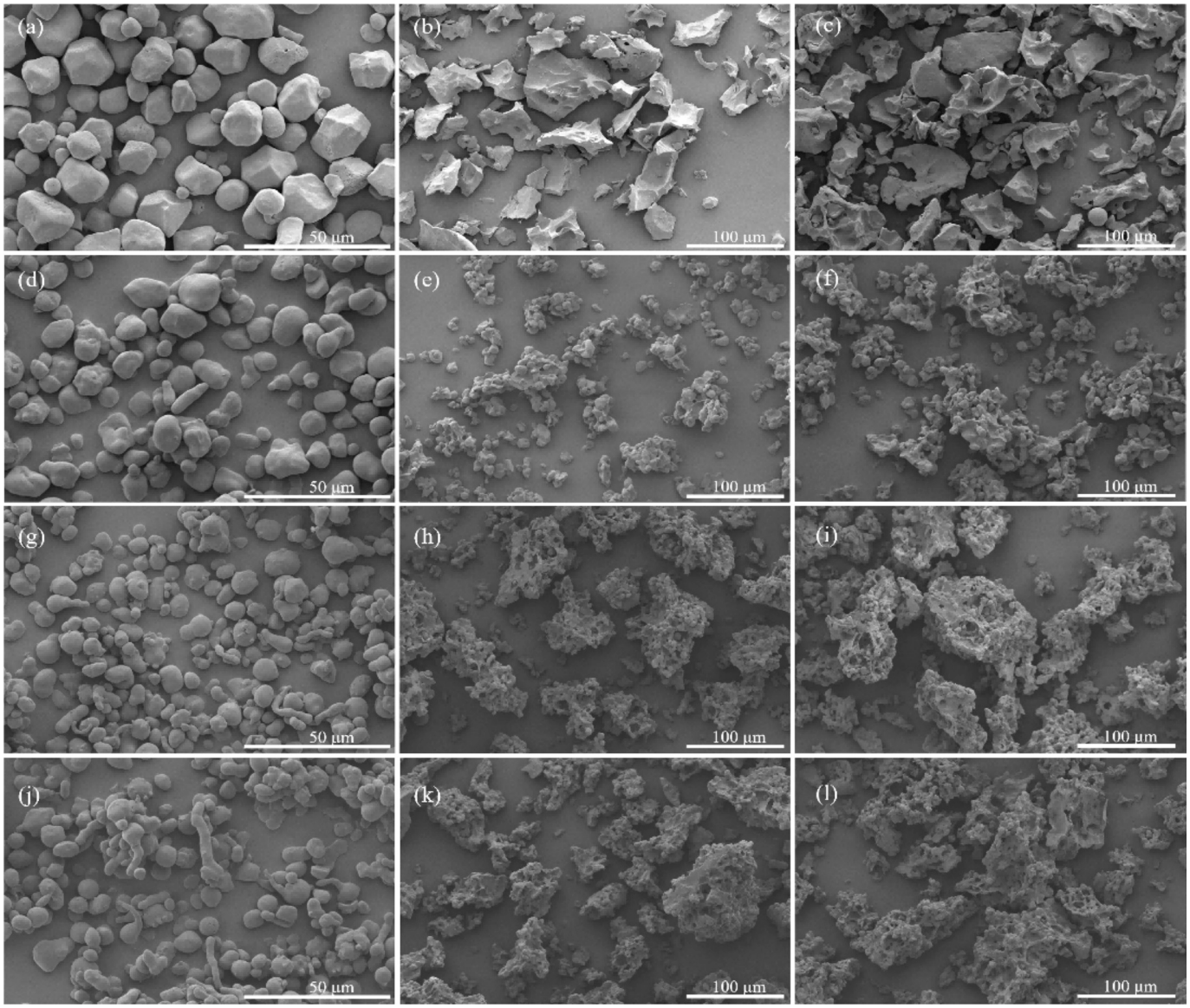

Fig. 5. SEM images of four native starches, gelatinized starches, and 3D-printed starches. (a) NS (3000×); (b) NS-G (1000×); (c) NS-D (1000×); (d) HACS-1946 (3000×); (e) HACS-1946-G (1000×); (f) HACS-1946-D (1000×); (g) HACS-K130 (3000×); (h) HACS-K130-G (1000×); (i) HACS-K130-D (1000×); (j) HACS-1945 (3000×); (k) HACS-1945-G (1000×); (l) HACS-1945-D (1000×).

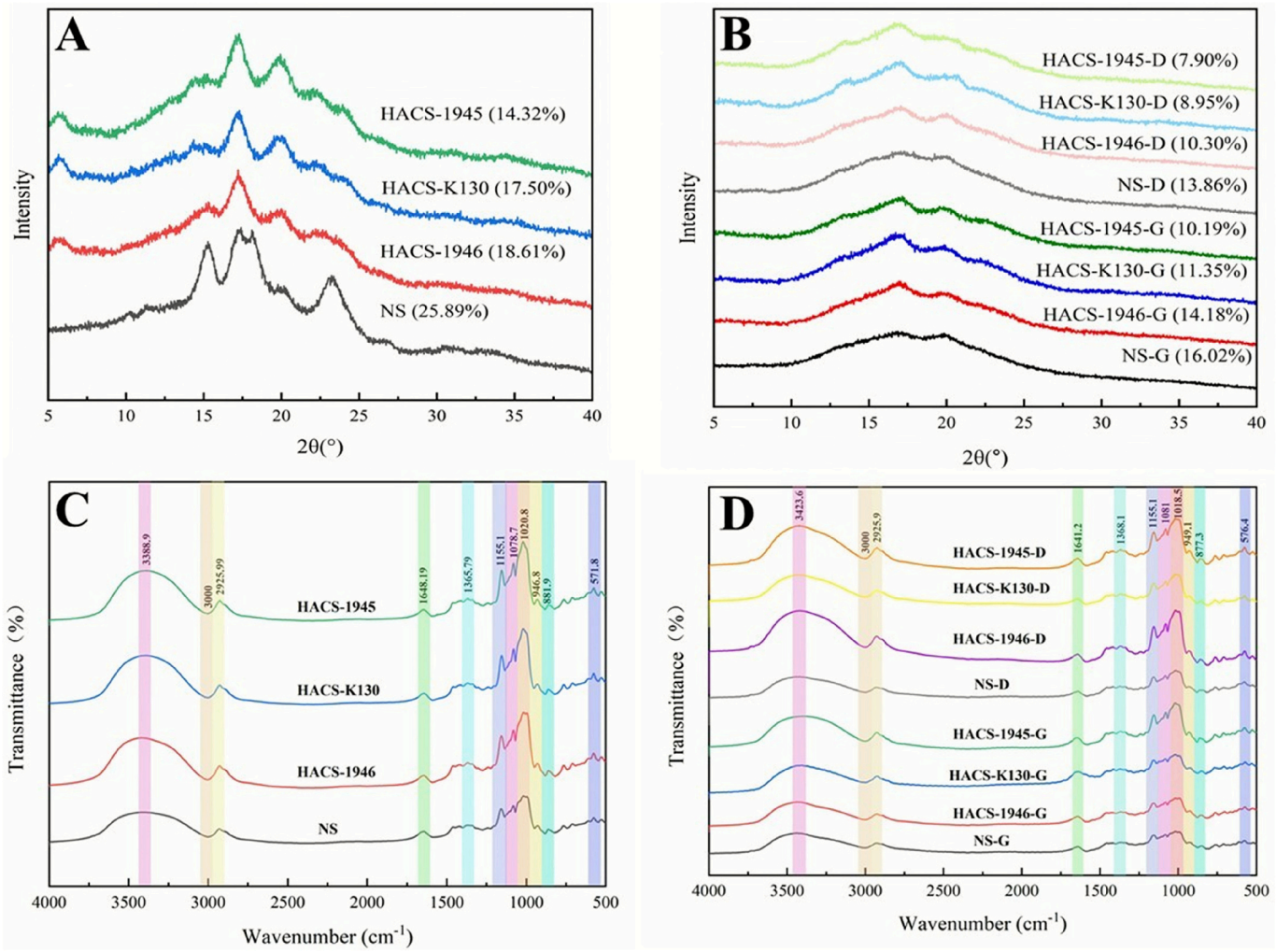

Fig. 6. XRD patterns and FTIR spectra of native, gelatinized, and 3D-printed corn starches. (A) XRD patterns of native corn starches; (B) XRD patterns of gelatinized and 3D-Printed corn starches. (C) FTIR spectra of native corn starches; (D) FTIR spectra of gelatinized and 3D-Printed corn starches.

dense structure, likely because the 3D printing process further densified the physical structure of the starch, thereby enhancing post-printing shape stability.

3.7. X-ray diffraction

X-ray diffraction (XRD) was a common method to evaluate the long-range order of starch samples.As shown in Fig. 6A and B, XRD patterns of four corn starches, gelatinized starches and 3D-printed starches. NS displayed a typical high-density A-type crystalline structure (compact double helix), characterized by strong diffraction peaks near 15°, 17°, 18°, and 23°, including connected double peaks around 17° and 18°. By contrast, HACS-1946, HACS-K130, and HACS-1945 exhibited B-type crystallinity (hydrated helical structure) with peaks at 5.6°, 15°, 17°, 19°, 22°. All native starches had a prominent peak at 20° (*V*-type structure from lipid-amylose interactions), with intensity increasing with amylose content. However, compared to native starch, gelatinized and 3D-printed starches showed only weak diffraction peaks near 17° and 20°, indicating gelatinization and 3D printing disrupted starch crystallinity.

The crystalline regions of starch were mainly composed of amylopectin molecules, while the amorphous regions consisted of amylose molecules. Higher amylopectin content correlated with greater relative crystallinity of the starch granules. Therefore, NS (25.89%) exhibited the highest relative crystallinity, indicating that more crystalline structures had to be disrupt during gelatinization. This finding was consistent with the DSC analysis results (Fig. 3A). Comparative analysis of native, gelatinized, and 3D-printed starches showed both processes reduced relative crystallinity. The gelatinization process disrupted the lamellar structure of starch granules and decreased the compactness of granule aggregates. Hydrothermal effects drove granules toward disorder, increasing the proportion of amorphous structures and reducing relative crystallinity. Extrusion damages starch crystalline regions, expanding amorphous areas (Ye et al., 2018). After complete gelatinization, starch primarily existed in an amorphous state, with starch chains showing high mobility. The 3D printing process may further disrupted the starch structure, hindering its ability to reorganize into ordered structures (Zheng et al., 2022).

3.8. Fourier transform infrared spectroscopy

As shown in Fig. 6C and D, FTIR spectra of native, gelatinized, and 3D-printed starches shared several characteristic peaks. The absorption band in the 3000–3600 cm^{-1} range was mainly attributed to O—H stretching vibrations and intermolecular hydrogen bond stretching vibrations. The peak near 2920 cm^{-1} represented the stretching vibration of CH_2. The absorption peak near 1640 cm^{-1} represented the characteristic stretching vibration of carbonyl groups (C=O). The 1470–1330 cm^{-1} peaks arose from C—H bending vibrations. Peaks at 1158, 1080, and 1024 cm^{-1} were mainly due to C—O stretching of C-O-H in starch

Table 5
Infrared spectral characteristic ratio of corn starch.

Sample	$R_{1047/1022}$	$R_{1022/995}$	Sample	$R_{1047/1022}$	$R_{1022/995}$	Sample	$R_{1047/1022}$	$R_{1022/995}$
NS	1.016 ± 0.001^{Aa}	0.984 ± 0.001^{Bc}	NS-G	0.961 ± 0.002^{Ab}	0.993 ± 0.001^{Bb}	NS-D	0.949 ± 0.003^{Ac}	0.996 ± 0.001^{Ba}
HACS-1946	1.008 ± 0.001^{Ba}	0.992 ± 0.001^{Ab}	HACS-1946-G	0.933 ± 0.003^{Cb}	1.003 ± 0.001^{Aa}	HACS-1946-D	0.907 ± 0.003^{Cc}	1.002 ± 0.001^{Aa}
HACS-K130	1.008 ± 0.000^{Ba}	0.924 ± 0.000^{Cc}	HACS-K130-G	0.947 ± 0.002^{Bb}	0.976 ± 0.001^{Cb}	HACS-K130-D	0.925 ± 0.003^{Bc}	0.992 ± 0.000^{Ca}
HACS-1945	1.004 ± 0.001^{Ca}	0.904 ± 0.004^{Dc}	HACS-1945-G	0.889 ± 0.001^{Dc}	0.966 ± 0.003^{Db}	HACS-1945-D	0.924 ± 0.001^{Bb}	0.996 ± 0.001^{Ba}

Note: Results are presented as mean ± standard deviation. Within a column of each group, data bearing different superscript letters indicate a significant difference. Differences between columns are indicated by capital letters in the table, while differences between rows are denoted by lowercase letters.

molecules. Meanwhile, peaks near 930, 860 and 572 cm^{-1} corresponded to the skeletal vibration of asymmetric ring modes (α-1,4-glycosidic bonds, C-O-C) (Zhang et al., 2024). The intensities of the peaks between 1100 and 900 cm-1 were different for native, gelatinized, or 3D-printed starches, which reflects a modification of the ordered region (995 and 1047 cm^{-1}) and the amorphous phase (1022 cm^{-1}) (Soler et al., 2020).

After gelatinisation and 3D printing processing, FTIR analysis of all starch samples demonstrated stable chemical structures, with no new characteristic absorption peaks detected. This observation reinforces the notion that both gelatinisation (high-temperature hydration expansion) and 3D printing (shear extrusion) are predominantly physical processes (Li et al., 2025). As shown in Table 5, the decreased 1047/1022 cm^{-1} ratio coupled with the increased 1022/995 cm^{-1} ratio in gelatinized starch, compared to its native counterpart, indicates a reduction in short-range molecular order and an expansion of amorphous regions. This structural alteration is primarily attributed to the thermal disruption of the amylopectin cluster structure during gelatinization. Concurrently, the leaching of amylose molecules into the amorphous domains further amplifies the structural disorder. This interpretation is consistent with findings reported by Wang et al. (2022), confirming that thermal treatment disrupts the ordered structure of starch. The subsequent extrusion shear during printing further disrupts the remaining ordered regions and inhibits molecular rearrangement during cooling. The molecular-scale order changes revealed by FTIR results correlate with the long-range crystallinity decline observed by XRD, confirming that heating gelatinisation, and printing exert a detrimental effect on the crystalline structure of starch.

3.9. In vitro starch digestibility

As shown in Table 6, with the increase in amylose content, the RS content in both native and gelatinised starch samples also gradually increased. The underlying reason is that increased amylose contributes to a differently structured starch granule matrix that does not hydrate efficiently, resulting in recalcitrant hydrolysis (Lv et al., 2021).

After gelatinization, the RS content of all starch samples decreased (e.g., NS-G, RS: 6.83%), indicating that high temperatures disrupted the crystalline regions of starch granules, causing amylose to leach out and form disordered structures that are more susceptible to enzymatic hydrolysis. The decrease in RS content was relatively smaller for HACS (e.g., HACS-1945-G, RS: 34.85%), due to partial resistant structures through rapid retrogradation after gelatinization. 3D-printed samples exhibited a further reduction in RS (e.g., HACS-1945-D, RS: 23.12%). This was primarily driven by extrusion shear, which disrupts starch granules, liberates molecular chains, and breaks interchain entanglements (Liu et al., 2021), thereby forming an open, porous network that significantly enhances enzyme accessibility and digestion efficiency. This mechanism is consistent with our XRD results, which showed a decrease in relative crystallinity following extrusion, a trend also reported by Yan et al. (2019).

The surface of Type A NS starch granules exhibits a naturally porous structure, This structure allows amylase molecules to penetrate directly, which facilitates efficient “inside-out” hydrolysis. The pore network structure formed after gelatinization further increases the enzyme-accessible surface area, leading to a significant increase in RDS content. The smooth, non-porous B-type HACS granules forced amylase to slowly hydrolyze only from the surface of the granules from the outside in (Obadi et al., 2023). Additionally, the dense molecular network formed by the high amylose content further slowed down the enzymatic hydrolysis rate. Although 3D printing partially disrupted the crystalline structure, the remaining fibrous entanglements still offered a certain level of enzyme resistance, leading to a higher RS content in HACS compared to NS.

As shown in Fig. 7, correlation analysis results indicate that amylose content exhibits positive correlations with G′, G″, gel hardness, and apparent viscosity. This indicates that high amylose content creates a three-dimensional network through hydrogen bonding between linear molecular chains, which contributes to the material's mechanical strength and elasticity. However, amylose content negatively correlates with tan δ and the height of the printed product. This indicates that during printing and stacking, the elasticity of high-amylose systems, which have weaker viscous dissipation, reduces layer height stability. This increases the risk of filament breakage or shrinkage in printed objects. Further analysis shows a positive correlation between amylose content and resistant starch content, while both negatively correlate with the starch's RC value and orderliness ($R_{1047/1022}$). No significant association exists between resistant starch content and rheological properties. This suggests that resistance to digestion relates to structural orderliness, while rheological characteristics influence printability, each governed by different mechanisms. These findings show that materials with high amylose content must sacrifice print accuracy and structural stability to improve mechanical properties and resistance to digestion.

Table 6
Rapidly digestible starch (RDS), slowly digestible starch (SDS), and resistant starch (RS) contents of corn starch.

Sample	RDS (%)	SDS (%)	RS (%)	Sample	RDS (%)	SDS (%)	RS (%)	Sample	RDS (%)	SDS (%)	RS (%)
NS	47.95 ± 0.37^{Ac}	41.96 ± 1.11^{Aa}	10.09 ± 0.74^{Ca}	NS-G	62.16 ± 1.66^{Ab}	31.01 ± 1.84^{Ab}	6.83 ± 0.18^{Db}	NS-D	65.81 ± 0.92^{Aa}	28.54 ± 1.29^{Ab}	5.66 ± 0.37^{Cb}
HACS-1946	44.70 ± 0.92^{Bb}	21.37 ± 2.95^{Ba}	33.93 ± 3.87^{Ba}	HACS-1946-G	52.78 ± 1.29^{Ba}	18.20 ± 0.68^{Ca}	29.02 ± 0.61^{Ca}	HACS-1946-D	54.74 ± 1.21^{Ba}	16.34 ± 0.68^{Ba}	28.92 ± 1.90^{Ba}
HACS-K130	26.40 ± 0.26^{Cc}	28.72 ± 0.29^{Bb}	44.88 ± 0.55^{Aa}	HACS-K130-G	40.79 ± 0.92^{Cb}	17.21 ± 0.01^{Cb}	42.01 ± 0.93^{Bab}	HACS-K130-D	43.91 ± 0.92^{Ca}	18.22 ± 1.50^{Ba}	37.86 ± 2.43^{Ab}
HACS-1945	23.03 ± 1.34^{Da}	29.58 ± 0.92^{Ca}	47.39 ± 0.42^{Aa}	HACS-1945-G	31.67 ± 1.29^{Da}	24.37 ± 1.29^{Bb}	43.97 ± 0.00^{Ab}	HACS-1945-D	35.75 ± 1.75^{Db}	25.89 ± 1.46^{Aab}	38.36 ± 1.29^{Ac}

Note: Results are presented as mean ± standard deviation. Within a column of each group, data bearing different superscript letters indicate a significant difference. Differences between columns are indicated by capital letters in the table, while differences between rows are denoted by lowercase letters.

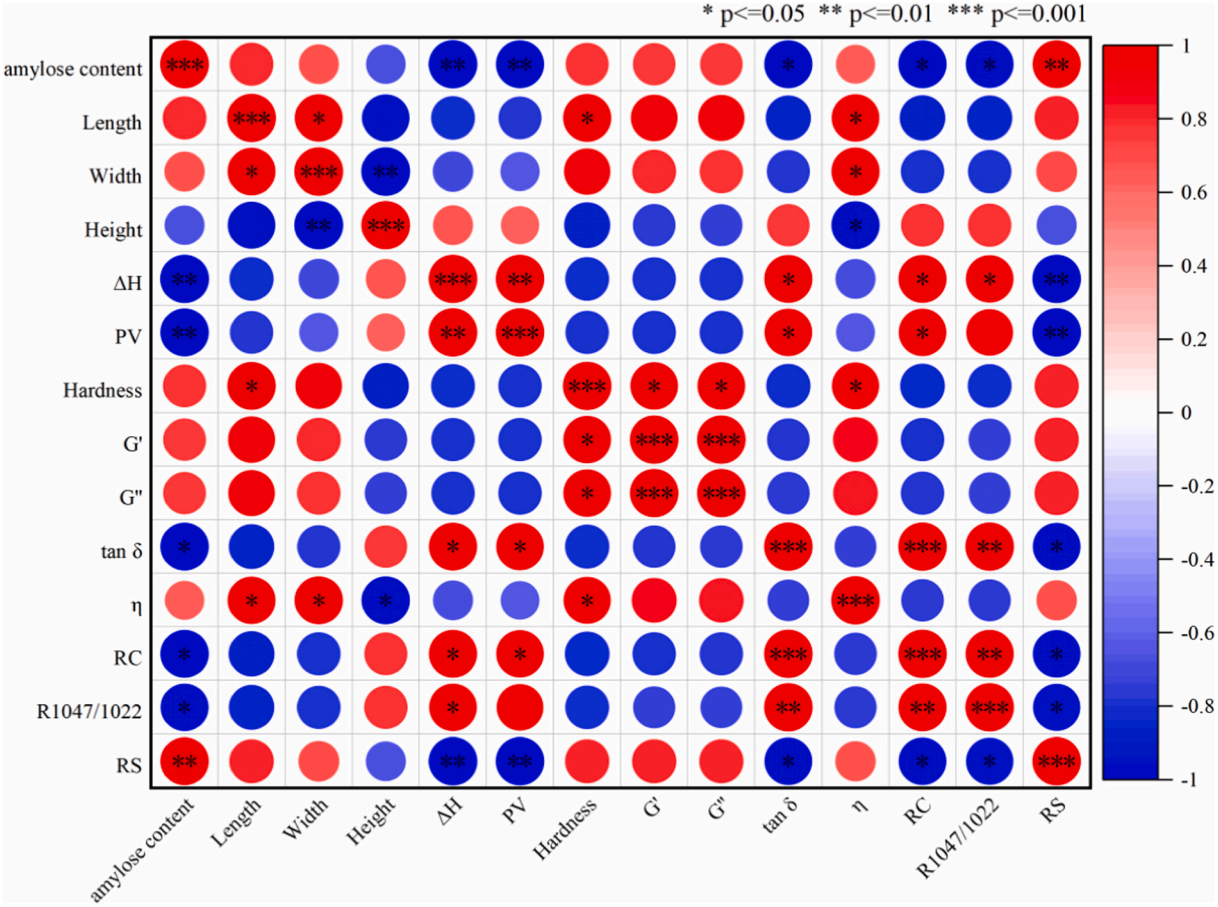

Fig. 7. Correlation between the geometric accuracy of 3D printed products and rheological properties. Rheological parameters were measured at a frequency of 1 Hz (G′, G″, and tan δ) and a shear rate of 1 s^{-1} (η).

This highlights the trade-off between printability and digestive functionality. The study's material, HACS-1946, supports this conclusion and offers a theoretical basis for selecting functional materials that combine good printability with high resistant starch content. This result provided new insights into developing 3D-printed foods that combine structural stability with controllable digestibility. By adjusting the amylose content and the parameters of the printing process, functional starch-based foods with a low glycemic index (GI) can be specifically designed.

4. Conclusion

The results show that amylose affects 3D printing performance in a nonlinear way. Not all high-amylose starches hinder printing. NS achieves optimal printing precision (with a deviation of less than 5%) due to its favorable particle characteristics and gel network. In contrast, HACS-K130 and HACS-1945 showed printing defects like poor extrusion flow and structural deformation caused by overly rigid gel networks. Correlation analysis shows that starch printability and resistance to digestion are influenced by different mechanisms. This offers a theoretical foundation for selecting functional materials that ensure good printability and high resistant starch content. XRD and FTIR results confirm that physical processing only changes starch's molecular arrangement without altering its chemical structure.Although NS exhibited the best printing accuracy, HACS-1946 (58.84% amylose) offered a superior balance between acceptable printability (6.59% deviation) and high digestion resistance (33.93% RS). These findings indicate that HACS-1946 is an ideal functional ink material for developing 3D-printed foods based on controllable digestible starch, with potential applications in areas such as low glycemic index (GI) foods. This study establishes key principles for screening and designing starch-based inks. These inks achieve high printing precision and controllable digestion characteristics. This research provides a scientific foundation for customizing food production.

CRediT authorship contribution statement

Ya'nan Wang: Writing – original draft, Supervision, Software, Methodology, Investigation, Formal analysis, Data curation, Conceptualization. **Shuangqi Tian:** Writing – review & editing, Supervision, Resources, Project administration, Funding acquisition, Conceptualization. **Mengsi Cui:** Writing – original draft, Investigation, Formal analysis. **Zixuan Liu:** Writing – original draft, Formal analysis. **Zhanpeng Liu:** Writing – original draft, Supervision, Investigation. **Zehua Liu:** Supervision, Investigation. **Jing Lu:** Supervision, Investigation.

Declaration of competing interest

The authors declare that they have no known competing financial interests or personal relationships that could have appeared to influence the work reported in this paper.

Acknowledgements

This research has been funded by the Henan Province International Science and Technology Cooperation Project (242102521003), the Henan Provincial Special Fund for the Construction of Modern Agricultural Industrial Technology System (No. HARS-22-02-G5), and the Science and Technology Innovation Leading Talent Program of Henan

Province (Grant No. 254200510031).

Data availability

Data will be made available on request.

References

Al-Muslimawi, A., Tamaddon-Jahromi, H. R., & Webster, M. F. (2013). Simulation of viscoelastic and viscoelastoplastic die-swell flows. *Journal of Non-Newtonian Fluid Mechanics, 191*, 45–56. https://doi.org/10.1016/j.jnnfm.2012.08.004

Bai, J., Dong, M., Li, J., Tian, L., Xiong, D., Jia, J., Yang, L., Liu, X., & Duan, X. (2022). Effects of egg white on physicochemical and functional characteristics of steamed cold noodles (a wheat starch gel food). *LWT - Food Science and Technology, 169*, Article 114057. https://doi.org/10.1016/j.lwt.2022.114057

Cai, L., Feng, L., Nie, M., Li, D., Zheng, T., & Zhang, M. (2023). Effect of different hydrocolloids on the rheological, microstructural, and 3D printing characteristics of purple sweet potato puree. *Food and Bioprocess Technology, 16*(4), 889–906. https://doi.org/10.1007/s11947-023-03085-2

Cheng, G., Gu, Z., Yang, Y., Wang, X., Zhao, R., Feng, Y., Huang, Q., & Jiang, H. (2024). Understanding resistant-starch formation during drying high-amylose maize kernels. *International Journal of Biological Macromolecules, 260*, Article 129419. https://doi.org/10.1016/j.ijbiomac.2024.129419

Cheng, Y., Fu, Y., Ma, L., Yap, P. L., Losic, D., Wang, H., & Zhang, Y. (2022). Rheology of edible food inks from 2D/3D/4D printing, and its role in future 5D/6D printing. *Food Hydrocolloids, 132*, Article 107855. https://doi.org/10.1016/j.foodhyd.2022.107855

Cheng, Y., He, Y., Xiao, L., Gao, W., Kang, X., Sui, J., & Cui, B. (2024). Impact of starch amylose and amylopectin on the rheological and 3D printing properties of corn starch. *International Journal of Biological Macromolecules, 134403*. https://doi.org/10.1016/j.ijbiomac.2024.134403

Cheng, Y., Liang, K., Chen, Y., Gao, W., Kang, X., Li, T., & Cui, B. (2023). Effect of molecular structure changes during starch gelatinization on its rheological and 3D printing properties. *Food Hydrocolloids, 137*, Article 108364. https://doi.org/10.1016/j.foodhyd.2022.108364

Cheng, Y., Yuqing, H., Xiao, L., Gao, W., Kang, X., Sui, J., & Cui, B. (2024). Impact of starch amylose and amylopectin on the rheological and 3D printing properties of corn starch. *International Journal of Biological Macromolecules, 134403*. https://doi.org/10.1016/j.ijbiomac.2024.134403

Dong, X., Pan, Y., Zhao, W., Huang, Y., Qu, W., Pan, J., Qi, H., & Prakash, S. (2020). Impact of microbial transglutaminase on 3D printing quality of Scomberomorus niphonius surimi. *LWT - Food Science and Technology, 124*, Article 109123. https://doi.org/10.1016/j.lwt.2020.109123

Englyst, H. N., Kingman, S. M., & Cummings, J. H. (1992). Classification and measurement of nutritionally important starch fractions. *European Journal of Clinical Nutrition, 46*, S33–S50. https://doi.org/10.1533/9781845698430.3.137

Fang, F., Luo, X., Fei, X., Michael Lim, J., Hamaker, B. R., & Campanella, O. H. (2020). Stored gelatinized waxy potato starch forms a strong retrograded gel at low pH with the formation of intermolecular double helices. *Journal of Agricultural and Food Chemistry, 68*(13), 4036–4041. https://doi.org/10.1021/acs.jafc.9b08268

Gu, Z., Sha, X., Wang, X., Zhao, R., Khashaba, R., Jane, J., & Jiang, H. (2024). Exploring characteristics of waxy wheat starches cross-linked at low levels: Insights from pasting, rheological, and textural properties. *Food Bioscience, 61*, Article 104672. https://doi.org/10.1016/j.fbio.2024.104672

Guan, C., Liu, J., Gan, S., Xiong, G., Qiao, F., Mo, W., Song, Y., Fu, X., Liu, C., & Lin, Q. (2023). Effects of soluble soybean polysaccharide on cooking and eating quality of dry rice noodles under single- and twin-screw extrusions. *LWT - Food Science and Technology, 187*, Article 115352. https://doi.org/10.1016/j.lwt.2023.115352

Gulzar, S., Narciso, J. O., Elez-Martínez, P., Martín-Belloso, O., & Soliva-Fortuny, R. (2023). Recent developments in the application of novel technologies for the modification of starch in light of 3D food printing. *Current Opinion in Food Science, 52*, Article 101067. https://doi.org/10.1016/j.cofs.2023.101067

Guo, K., Tian, Y., Podzimska-Sroka, D., Kirkensgaard, J. J. K., Herburger, K., Enemark-Rasmussen, K., … Zhong, Y. (2024). Structural evolution of maize starches with different amylose content during pasting and gelation as evidenced by rapid Visco analyser. *Food Chemistry, 461*, Article 140817. https://doi.org/10.1016/j.foodchem.2024.140817

He, C., Zhang, M., & Fang, Z. (2020). 3D printing of food: Pretreatment and post-treatment of materials. *Critical Reviews in Food Science and Nutrition, 60*(14), 2379–2392. https://doi.org/10.1080/10408398.2019.1641065

Jiang, H., Campbell, M., Blanco, M., & Jane, J.-L. (2010). Characterization of maize amylose-extender (ae) mutant starches: Part II. Structures and properties of starch residues remaining after enzymatic hydrolysis at boiling-water temperature. *Carbohydrate Polymers, 80*(1), 1–12. https://doi.org/10.1016/j.carbpol.2009.10.060

Jiang, H., Zheng, L., Zou, Y., Tong, Z., Han, S., & Wang, S. (2019). 3D food printing: Main components selection by considering rheological properties. *Critical Reviews in Food Science and Nutrition, 59*(14), 2335–2347. https://doi.org/10.1080/10408398.2018.1514363

Jiang, L., Wang, C., Zhang, F., Cui, K., Wang, Y., Dong, B., Tian, J., & Jiang, H. (2025). Understanding properties and digestibility of starch sodium octenyl succinate derived from high-amylose wheat starch. *Carbohydrate Polymers, 358*, Article 123512. https://doi.org/10.1016/j.carbpol.2025.123512

Jo, G. H., Lim, W. S., Kim, H. W., & Park, H. J. (2021). Post-processing and printability evaluation of red ginseng snacks for three-dimensional (3D) printing. *Food Bioscience, 42*, Article 101094. https://doi.org/10.1016/j.fbio.2021.101094

Kaur, P., Kaur, K., Basha, S. J., & Kennedy, J. F. (2022). Current trends in the preparation, characterization and applications of oat starch — A review. *International Journal of Biological Macromolecules, 212*, 172–181. https://doi.org/10.1016/j.ijbiomac.2022.05.117

Li, C., Hu, Y., & Li, E. (2021). Effects of amylose and amylopectin chain-length distribution on the kinetics of long-term rice starch retrogradation. *Food Hydrocolloids, 111*, Article 106239. https://doi.org/10.1016/j.foodhyd.2020.106239

Li, Q., Ma, L., Liu, J., Cheng, Y., & Liang, J. (2025). The multiscale structural properties and in-vitro digestibility of high amylose corn starch during autoclaving-cooling treatment. *Starch - Stärke., 77*(1), Article 2300250. https://doi.org/10.1002/star.202300250

Liu, B., Zhao, Y., Li, Y., Tao, L., Pan, P., Bi, Y., Song, S., & Yu, L. (2024). Investigation of the structure, rheology and 3D printing characteristics of corn starch regulated by glycyrrhizic acid. *International Journal of Biological Macromolecules, 263*, Article 130277. https://doi.org/10.1016/j.ijbiomac.2024.130277

Liu, P., Ling, J., Mao, T., Liu, F., Zhou, W., Zhang, G., & Xie, F. (2023). Adhesive and flame-retardant properties of starch/Ca2+ gels with different amylose contents. *Molecules, 28*(11), 4543. https://doi.org/10.3390/molecules28114543

Liu, Q., Chen, P., Li, P., Zhao, J., Olnood, C. G., Zhao, S., … Chen, X. (2023). Effects of Salecan on the gelatinization and retrogradation behaviors of wheat starch. *LWT - Food Science and Technology, 186*, Article 115238. https://doi.org/10.1016/j.lwt.2023.115238

Liu, Z., Bhandari, B., Prakash, S., Mantihal, S., & Zhang, M. (2019). Linking rheology and printability of a multicomponent gel system of carrageenan-xanthan-starch in extrusion based additive manufacturing. *Food Hydrocolloids, 87*, 413–424. https://doi.org/10.1016/j.foodhyd.2018.08.026

Liu, Z., Bhandari, B., Prakash, S., & Zhang, M. (2018). Creation of internal structure of mashed potato construct by 3D printing and its textural properties. *Food Research International, 111*, 534–543. https://doi.org/10.1016/j.foodres.2018.05.075

Liu, Z., Yang, J., Shi, Z., Chen, L., & Zheng, B. (2021). Effect of stearic acid on the microstructural, rheological and 3D printing characteristics of rice starch. *International Journal of Biological Macromolecules, 189*, 590–596. https://doi.org/10.1016/j.ijbiomac.2021.08.174

Lv, X., Hong, Y., Zhou, Q., & Jiang, C. (2021). Structural features and digestibility of corn starch with different amylose content. *Frontiers in Nutrition, 8*, Article 692673. https://doi.org/10.3389/fnut.2021.692673

Masbernat, L., Berland, S., Leverrier, C., Moulin, G., Michon, C., & Almeida, G. (2021). Structuring wheat dough using a thermomechanical process, from liquid food to 3D-printable food material. *Journal of Food Engineering, 310*, Article 110696. https://doi.org/10.1016/j.jfoodeng.2021.110696

Meng, F., Tian, S., Chen, Y., & Liu, Z. (2025). Preparation and physicochemical properties of OSA modified Cyperus esculentus starch nanoparticles. *International Journal of Biological Macromolecules, 140045*. https://doi.org/10.1016/j.ijbiomac.2025.140045

Ning, J., Fu, B., Tang, X., Hao, Y., Zhang, Y., & Wang, X. (2025). Starch retrogradation in starch-based foods: Mechanisms, influencing factors, and mitigation strategies. *International Journal of Biological Macromolecules, 300*, Article 140354. https://doi.org/10.1016/j.ijbiomac.2025.140354

Obadi, M., Qi, Y., & Xu, B. (2023). High-amylose maize starch: Structure, properties, modifications and industrial applications. *Carbohydrate Polymers, 299*, Article 120185. https://doi.org/10.1016/j.carbpol.2022.120185

Rong, L., Chen, X., Shen, M., Yang, J., Qi, X., Li, Y., & Xie, J. (2023). The application of 3D printing technology on starch-based product: A review. *Trends in Food Science & Technology, 134*, 149–161. https://doi.org/10.1016/j.tifs.2023.02.015

Shi, S., Wen, J., Geng, H., Zhan, X., & Liu, Y. (2024). Physicochemical properties, structural properties and gels 3D printing properties of wheat starch. *International Journal of Biological Macromolecules, 261*, Article 129885. https://doi.org/10.1016/j.ijbiomac.2024.129885

Soler, A., Mendez-Montealvo, G., Velazquez-Castillo, R., Hernández-Gama, R., Osorio-Diaz, P., & Velazquez, G. (2020). Effect of crystalline and double helical structures on the resistant fraction of autoclaved corn starch with different amylose content. *Starch - Stärke, 72*(11−12), Article 1900306. https://doi.org/10.1002/star.201900306

Tian, Y., Wang, Y., Herbuger, K., Petersen, B. L., Cui, Y., Blennow, A., … Zhong, Y. (2023). High-pressure pasting performance and multilevel structures of short-term microwave-treated high-amylose maize starch. *Carbohydrate Polymers, 322*, Article 121366. https://doi.org/10.1016/j.carbpol.2023.121366

Wang, H., Li, Y., Wang, L., Wang, L., Li, Z., & Qiu, J. (2022). Multi-scale structure, rheological and digestive properties of starch isolated from highland barley kernels subjected to different thermal treatments. *Food Hydrocolloids, 129*, Article 107630. https://doi.org/10.1016/j.foodhyd.2022.107630

Wei, Z., Cheng, L., Hong, Y., Li, Z., Li, C., Ban, F., & Gu, Z. (2025). Complexation behavior and physicochemical properties of maize starch–linolenic acid complexes prepared using corn starch with different amylose contents through extrusion. *International Journal of Biological Macromolecules, 144239*. https://doi.org/10.1016/j.ijbiomac.2025.144239

Wen, J.-J., Li, M.-Z., Hu, J.-L., Tan, H.-Z., & Nie, S.-P. (2022). Resistant starches and gut microbiota. *Food Chemistry, 387*, Article 132895. https://doi.org/10.1016/j.foodchem.2022.132895

Yan, X., Wu, Z.-Z., Li, M.-Y., Yin, F., Ren, K.-X., & Tao, H. (2019). The combined effects of extrusion and heat-moisture treatment on the physicochemical properties and

digestibility of corn starch. *International Journal of Biological Macromolecules, 134*, 1108–1112. https://doi.org/10.1016/j.ijbiomac.2019.05.112

Ye, J., Hu, X., Luo, S., Liu, W., Chen, J., Zeng, Z., & Liu, C. (2018). Properties of starch after extrusion: A review. *Starch - Stärke, 70*(11–12), Article 1700110. https://doi.org/10.1002/star.201700110

You, S., Huang, Q., & Lu, X. (2023). Development of fat-reduced 3D printed chocolate by substituting cocoa butter with water-in-oil emulsions. *Food Hydrocolloids, 135*, Article 108114. https://doi.org/10.1016/j.foodhyd.2022.108114

Yu, S., Liu, J., Yang, Y., Ren, J., Zheng, X., & Kopparapu, N. K. (2016). Effects of amylose content on the physicochemical properties of Chinese chestnut starch. *Starch - Stärke, 68*(1–2), 112–118. https://doi.org/10.1002/star.201500177

Zhang, R.-Y., Chen, P.-X., Liu, A.-B., Zhu, W.-X., Jiang, M.-M., Wang, X.-D., & Liu, H.-M. (2024). Effects of different isolation methods on the structure and functional properties of starch from tiger nut (Cyperus esculentus L.) meal. *LWT - Food Science and Technology, 196*, Article 115853. https://doi.org/10.1016/j.lwt.2024.115853

Zhang, S., Fu, Q., Li, H., Li, Y., Wu, P., & Ai, S. (2024). Polydopamine-coated lignin nanoparticles in polysaccharide-based films: A plasticizer, mechanical property enhancer, anti-ultraviolet agent and bioactive agent. *Food Hydrocolloids, 147*, Article 109325. https://doi.org/10.1016/j.foodhyd.2023.109325

Zheng, B., Tang, Y., Xie, F., & Ling, C. (2022). Effect of pre-printing gelatinization degree on the structure and digestibility of hot-extrusion 3D-printed starch. *Food Hydrocolloids, 124*, Article 107210. https://doi.org/10.1016/j.foodhyd.2021.107210

Zhong, Y., Qu, J., Li, Z., Tian, Y., Zhu, F., Blennow, A., & Liu, X. (2022). Rice starch multi-level structure and functional relationships. *Carbohydrate Polymers, 275*, Article 118777. https://doi.org/10.1016/j.carbpol.2021.118777

Zhong, Y., Tai, L., Blennow, A., Ding, L., Herburger, K., Qu, J., … Liu, X. (2023). High-amylose starch: Structure, functionality and applications. *Critical Reviews in Food Science and Nutrition, 63*(27), 8568–8590. https://doi.org/10.1080/10408398.2022.2056871